Probing Neural Networks for Dynamic Switches of Communication Pathways

Holger Finger[a,b,1,2], Richard Gast[b,c,1], Christian Gerloff[d], Andreas K. Engel[a], Peter König[a,b]

a Department of Neurophysiology and Pathophysiology, University Medical Center Hamburg-Eppendorf, Hamburg
b Institute of Cognitive Science, University of Osnabrück, Osnabrück
c MPI for Human Cognitive and Brain Sciences, Leipzig
d Department of Neurology, University Medical Center Hamburg-Eppendorf, Hamburg

1 Contributed equally to this work.
2 holger.finger@uni-osnabrueck.de

Abstract

Communication and dynamic routing play important roles in the human brain to facilitate flexibility in task solving and thought processes. Here, we present a new network perturbation methodology and a corresponding analysis method to investigate and demonstrate the dynamic switching between different excitable pathways in the network. The methodology probes for dynamic changes in network communication pathways based on the relative phase offsets between two weak external oscillatory drivers. To investigate the feasibility and the properties of this method we use a computational modeling approach with delay-coupled neural mass models. In a model of the human connectome we show that network pathways have characteristic timescales and thus specific preferences for the phase lag between the regions they connect. For the analysis of dynamic switches of communication pathways we define the pathway-synchronization-facilitation index (PSF), which measures for a given pair of network nodes how their interaction is modulated by specific phase offsets. Our simulation results indicate that the PSF decreases with increasing shortest path length between the node-pair and increases with the number of different pathways by which the two nodes are connected. To further analyze the contribution of different interaction pathways to the communication between two network nodes, we define the pathway-activation index (PA). Our results show that most pairs of nodes in the connectome have interaction pathways that can be dynamically activated and that 60.1% of node pairs can switch their communication from one pathway to another depending on the phase offsets between the two nodes.

Significance

A big challenge in elucidating information processing in the brain is to understand the neural mechanisms that dynamically organize the communication between different brain regions in a flexible and task-dependent manner. In this theoretical study, we present an approach to investigate the routing and gating of information flow along

different pathways from one region to another. We show that stimulation of the brain at two sites with different frequencies and oscillatory phases can reveal the underlying effective connectivity. This yields new insights into the underlying processes that govern dynamic switches in the communication pathways between remote sites of the brain.

Introduction

Over the past decades it has been shown that the brain, facing a specific task or not, reveals a well-structured functional organization [4, 6, 29]. This has been specifically investigated for resting-state networks [2, 5, 9, 24], but also for other networks when the brain is performing different tasks [5, 17]. These findings lead to the idea that resting-state networks describe an inherent functional organization of the brain which is optimized to perform a wide range of tasks it encounters frequently [11, 15]. If faced with a task that requires synchronization between brain areas not typically coupled at rest, this organization has to be altered temporarily in order to perform that task efficiently [18, 26].

Within a complex network like the human brain, multiple structural pathways exist between most pairs of nodes given a sufficiently high spatial resolution. Since synchronization along such pathways seems to play an important role in the formation of functional clusters, we set out to identify general principles of how these pathways interact with each other during synchronization processes. Several studies have emphasized the importance of information transmission delay for synchronization processes as well as its role in the formation of functional clusters in the brain [3, 4, 7, 8, 12, 14, 16, 28]. Thus, we hypothesize the time lag inherent to a communication path to be a key factor in the interaction between multiple pathways. These time windows are determined by axonal signal transmission delays as well as rise and decay properties of the post-synaptic response. Here, we focus on the former, expecting region-specific differences in the latter to be negligible for the long-range connections considered in this study. In particular, we predict that two brain regions trying to communicate at a certain frequency with a given phase offset will use only a fraction of their available communication paths. Further, we predict that the selection of communication paths will be influenced by their interaction time windows.

To test these hypotheses, we introduce an extrinsic stimulation set-up that allows to detect network interactions between pairs of nodes. This stimulation approach relies on the entrainment of a given pair of nodes to oscillate at the same frequency, but with a certain phase lag relative to each other. Comparing the coherence along different pathways over different stimulation phase offsets then reveals the phase preferences for different routes. While Figure 1A illustrates the extrinsic stimulation setup, Figure 1B motivates the use of different stimulation phase lags. It is important to note that even in the absence of any interaction through the network, there might be some induced trivial coherence between two stimulated nodes due to the external signal (Figure 1B). Thus, the coherence is measured for many different stimulation phase offsets and the measurement with the lowest coherence is chosen as the baseline. Any deviation in the coherence from this baseline can be attributed to induced changes in the coupling between the two stimulated nodes through the network, which may happen due to a switching in the pathways (compare Figure 1C and 1D). We propose that these differences in phase preferences at different pathways act as a switching and gating mechanism used by the brain to establish communication between remote brain areas when needed. Our method allows to investigate these mechanisms by probing the network for these dynamic switches in communication pathways.

In the next section, we define the computational model used for the evaluation of this methodology. We continue by demonstrating the phase offset preferences of

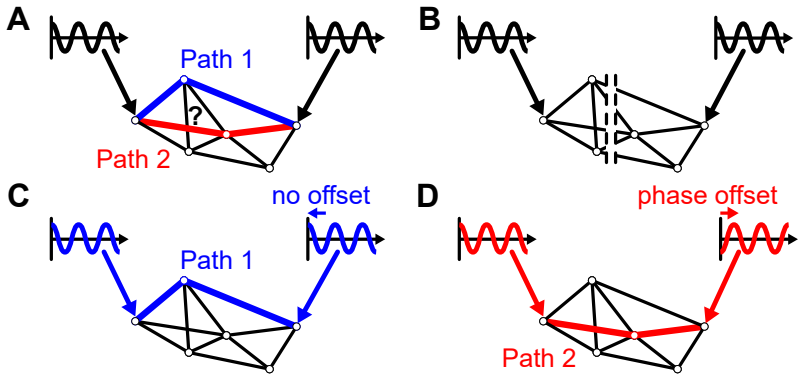

Figure 1. Illustration of the stimulation methodology and different possible outcomes. (A) The stimulation at the two nodes could potentially activate different paths (blue or red) in the network. (B) As an alternative explanation it could also be possible that a coherence between the two nodes is induced even in the absence of any direct interaction in the network. (C) In this example a stimulation phase offset of 0π induces a network interaction between the two stimulated nodes through path 1 (blue). (D) In contrast, when stimulating with a phase offset of π another path is activated (red).

different pathways in a simplified network of only 2-3 nodes. Subsequently, we move on to a human connectome model and show that coherence between stimulated nodes changes significantly over phase lags and how this effect relates to the connectedness and distance of the nodes. In a final step, we identify the pathways responsible for the interaction between the stimulated nodes, analyze their phase lag preferences and identify cases of phase-related switching between pathways. To this end, we evaluate how the activation of predefined structural pathways between stimulated nodes changes over different stimulation phase offsets.

Computational Model

To investigate switching and gating properties of networks based on phase relationships, we employ the computational model described in this section. Our computational model is based on the widely used Jansen-Rit neural mass model [21] which employs a mean-field approach to model the interaction between cell populations in the infragranular (green), granular (blue), and supragranular (red) layer, as illustrated with the relevant equations in Figure 2. The standard parametrization originally proposed by Jansen and Rit reflects cortical oscillatory activity in the alpha frequency band. Since the purpose of this article is the investigation of the effect of pathway time-scales on neural synchronization processes and not the effect of node time-scales, we decided to use this standard parametrization for each node in our network [21]. These parameters were chosen based on experimental findings in the neuroscience literature and are reported in Table S1 in the SI Appendix together with the definition of the transformation function $\sigma(V)$ from average membrane potentials to firing rates (parameterized sigmoid).

To obtain the results reported below, the following two extensions were added to the standard Jansen-Rit model: First, we coupled multiple Jansen-Rit nodes via delayed, weighted connections between their infragranular pyramidal cell populations (yellow in Figure 2). Secondly, weak external drivers were applied at two stimulation sites influencing the average membrane potential of the infragranular layer with phase offset $\Delta\varphi$ between the two drivers (purple in Figure 2).

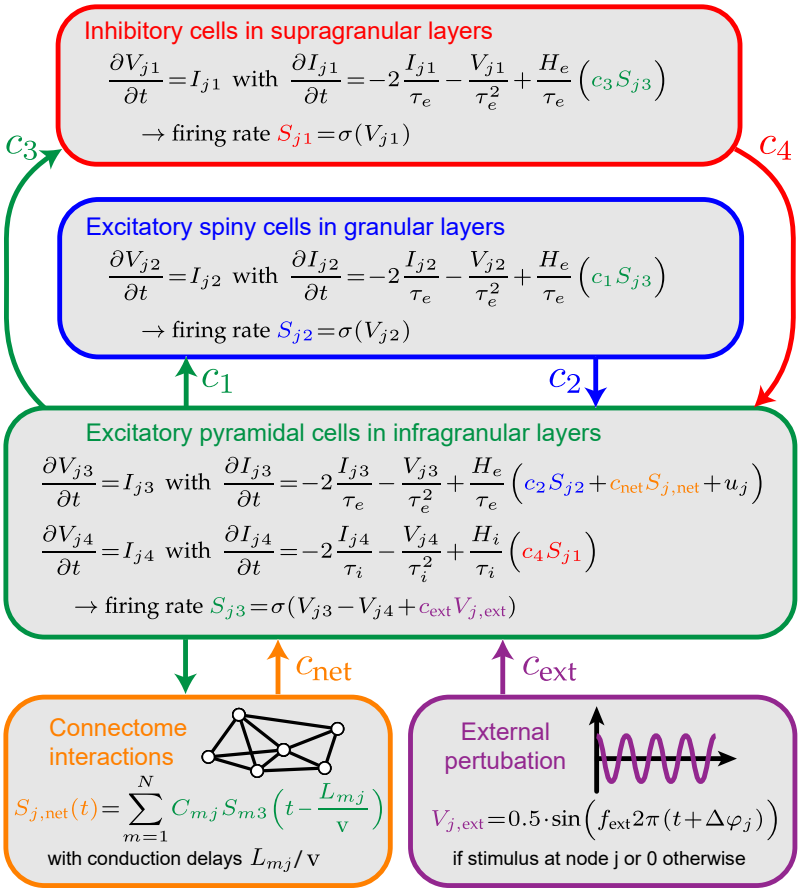

Figure 2. Neural mass model with external stimulation. A schematic of the neural mass model showing the interactions between the three neuronal populations in the infragranular, granular, and supragranular layer. Each post-synaptic potential is modeled using two differential equations (average membrane potentials V and average synaptic currents I. Several of these neural mass models are interacting through a connectivity matrix (yellow). The external perturbation (purple) modulates the average membrane potential of pyramidal cells at 2 nodes in the network.

Results

We first present results of simple simulations with only 2 or 3 nodes. Specifically, we show how the coherence depends on the transmission delay of the connections and on the relative phase offsets between the two external signals. Subsequently, we move on to the connectome simulation, where we first evaluate the overall similarity of the simulated functional connectivity with the functional connectivity obtained from electroencephalography (EEG) recordings. Finally, we present results of the connectome simulation showing a dependence of network communication on the stimulation protocol and the characteristic time-scales of communication paths.

Simple Models With 2 or 3 Nodes

The idea behind the extrinsic stimulation approach can be well explained using a simple toy-model of 2 directly coupled Jansen-Rit nodes, where each node is stimulated with a $f_{\text{ext}} = 11$ Hz sinusoidal signal with strength $c_{\text{ext}} = 0.25$ mV. Figure 3 shows the

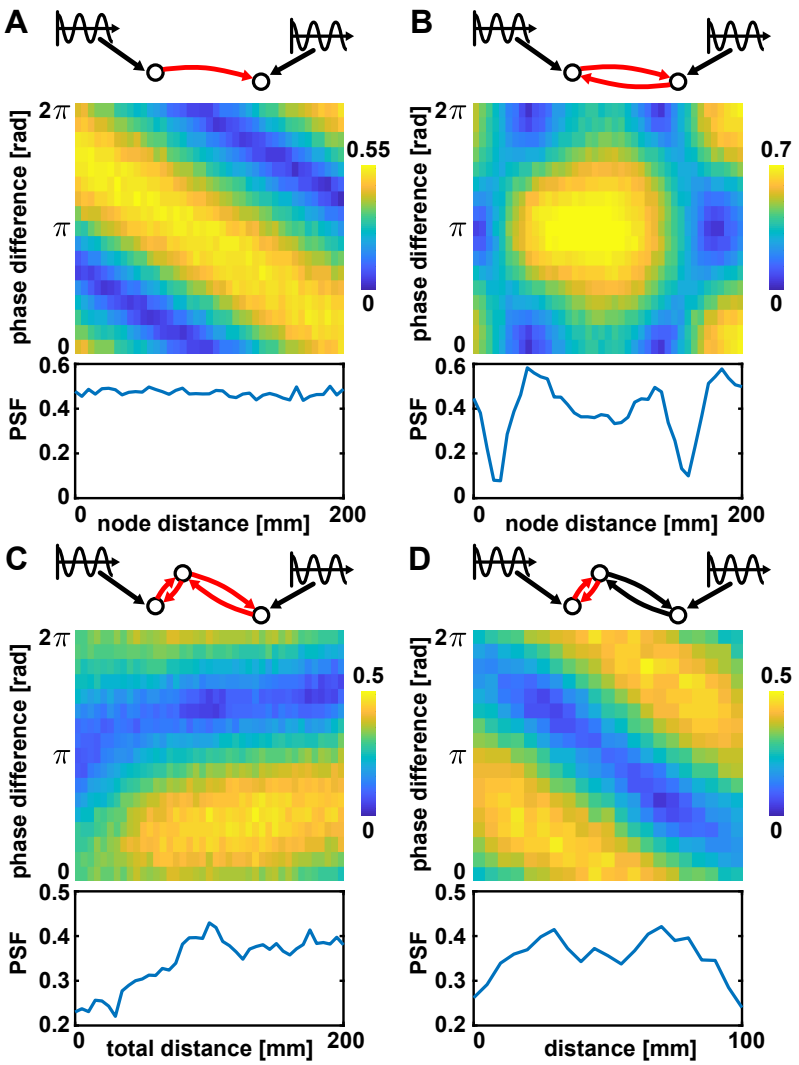

Figure 3. Simulations with 2 or 3 nodes, where the red edges correspond to the distance that was varied. Color indicates the coherence between the two driven nodes. The PSF values are shown at the bottom of each panel. (A) Nodes with direct uni-directional coupling. (B) Nodes with direct bi-directional coupling. (C) Nodes with indirect (via a third node) bi-directional couplings. The intermediate node was placed at 25 % of the total connection distance, while the overall distance between the outer nodes was varied. (D) Nodes with indirect bi-directional couplings where the overall distance was kept at 100 mm, while the intermediate node was positioned at varying positions along the connection. Parameters used in all panels: $v = 3$ m/s, $C_{mj} \cdot c_{\text{net}} = 0.1$ if there is a connection from node m to j or 0 otherwise.

coherence between the driven nodes for systematic changes in the phase offset between the stimuli and the distance between the coupled nodes. While uni-directionally coupled nodes can have preferences for any stimulation phase offset, as shown in Figure 3A, bi-directionally coupled nodes are more susceptible for stimulation at in- or anti-phase (see Figure 3B). This shows that the communication between coupled pairs of nodes can be modulated by stimulation and that communication channels can have characteristic stimulation phase offset preferences, depending on their length [22].

To quantify the modulation of communication, we define the pathway-synchronization-facilitation (PSF), measuring for a given pair of weakly stimulated network nodes k_i and k_j how their interaction is dependent on specific phase offsets:

$$\mathrm{PSF}(k_i, k_j) = \max_{0 \le \Delta\varphi \le 2\pi} \Big(\mathrm{coh}(k_i, k_j, \Delta\varphi) \Big) - \min_{0 \le \Delta\varphi \le 2\pi} \Big(\mathrm{coh}(k_i, k_j, \Delta\varphi) \Big), \quad (1)$$

where $\mathrm{coh}(k_i, k_j, \Delta\varphi)$ is the coherence between network nodes k_i and k_j for stimulation phase offset $\Delta\varphi$. The PSF is high for node pairs if their coherence is high for one stimulation phase offset and low for another, i.e., the relative phase of the stimulation at the two sites matters strongly. The PSF curves in Figure 3A and 3B show that in both cases there is a PSF effect (PSF ¿ 0) and in the case of bi-directionally coupled nodes the strength of this effect depends on the distance between the nodes.

To extend this idea to communication via indirect pathways, we investigated synchronization between 2 nodes connected only indirectly via a third intermediate node. We used bi-directional couplings for both connections and both end nodes were stimulated as described previously. As can be seen in Figure 3C and 3D, the interaction between the two weakly stimulated nodes not only depended on the length of the connection, but potentially also on the relative position of the third node on the indirect path.

Connectome Model Without Stimulation

As shown in the previous section, the coherence in a network of only three nodes can already exhibit very complex dependencies on the stimulation phase offset. Next, we wanted to analyze network communication patterns in the case of a complex network with multiple competing pathways. To this end, we used a model of 33 delay-connected nodes, representing one hemisphere of the human connectome [14]. The structural connectivity matrix was obtained from diffusion tensor imaging (DTI) data as described in more detail in the SI Appendix. Figure 4A shows the sparse connectivity matrix C_{mj} used to connect the 33 regions and Figure 4B the corresponding distances L_{mj}.

For the same 33 regions, EEG resting-state recordings from the same subjects were used to calculate pairwise coherences in the 10 Hz range as shown in Figure 4C (details in SI Appendix). Similarly, we simulated the 33 connected neural-mass-models and processed the time-series of the pyramidal cells in the same way as the EEG data. This yielded a 33 x 33 functional connectivity matrix which we compared to the empirical functional connectivity by calculating the Pearson correlation coefficient.

The selection of parameters was based on the rationale to match the functional connectivity observed in the network model as good as possible to empirical EEG-based functional connectivity from human subjects. We performed a grid search over global structural connectivity scaling c_{net} and transmission velocity v to obtain the best match between modeled and empirical data. By fitting the velocity, we ensured that our pathway delays reflect realistic, empirically observed timescales of cortico-cortical interactions. We found the highest correlation (r = 0.57) for $c_{\mathrm{net}} = 20$ and v = 3 m/s, so that we used these parameters for subsequent analyses (Figure 4D). Notice that this correlation is comparable with values of other bottom-up models reported in the literature [14, 25], which is remarkable considering that we set a substantial amount of structural connections to 0.

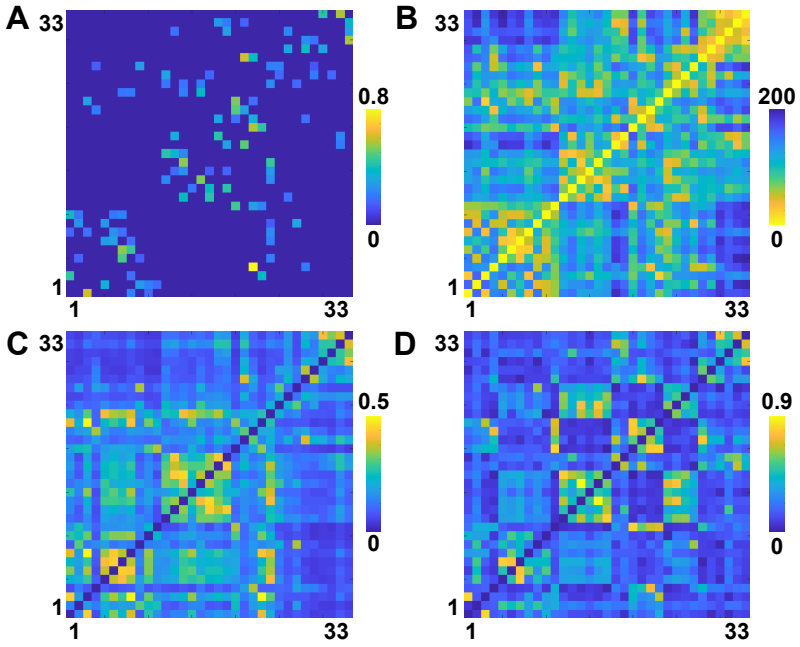

Figure 4. Pairwise measures of connectivity and distance between all 33x33 region pairs. (A) Structural connectivity matrix with all connections smaller 0.1 set to 0. (B) Inter-regional distances in mm. (C) Functional connectivity matrix derived from coherence of EEG data bandpass-filtered around 10 Hz. (D) Functional connectivity derived from coherence of neural mass model simulations bandpass-filtered around 10 Hz.

Connectome Model With Stimulation

Based on this model of cortical activity we used the stimulation approach to investigate how pathways facilitate synchronization between network nodes at certain phase lags between the nodes. Specifically, we weakly stimulated different pairs of cortical regions with varying phase offsets between the two stimulation signals while measuring the coherence between the stimulated nodes at each phase offset. As argued above, finding differences in the coherence over stimulation phase offsets would indicate phase-specific communication modulation between the stimulated nodes. Before analyzing PSF effects in the connectome model, it was necessary to determine the optimal stimulation frequency and strength for this model. This was performed in two steps. First, we stimulated a single region in our network with a stimulus of varying frequency (4-22 Hz) and strength (0.01-2 mV) while evaluating the coherence between region and stimulus. The mean coherence (mean over 5 different stimulated nodes) for each parameter combination can be observed in Figure 5A. Since our main analysis will focus on coupling effects through different network paths between two stimulated nodes, we also calculated the coherence between stimulus and all network nodes (Figure 5B). This average coherence to the full network was strongest at 9-11 Hz, which is also the intrinsic frequency of unperturbed network nodes [27]. Interestingly, at this frequency the coherence to the directly stimulated node was weakest (compare 5A). Based on this, we set the frequency of our stimulus to 11 Hz, at which the network (and not only the directly stimulated node) was most susceptible for entrainment by an external stimulation.

In a second step, we stimulated pairs of nodes with 11 Hz stimuli. We varied the stimulus strength (0.25 - 1 mV) and the relative phase offset between the stimuli

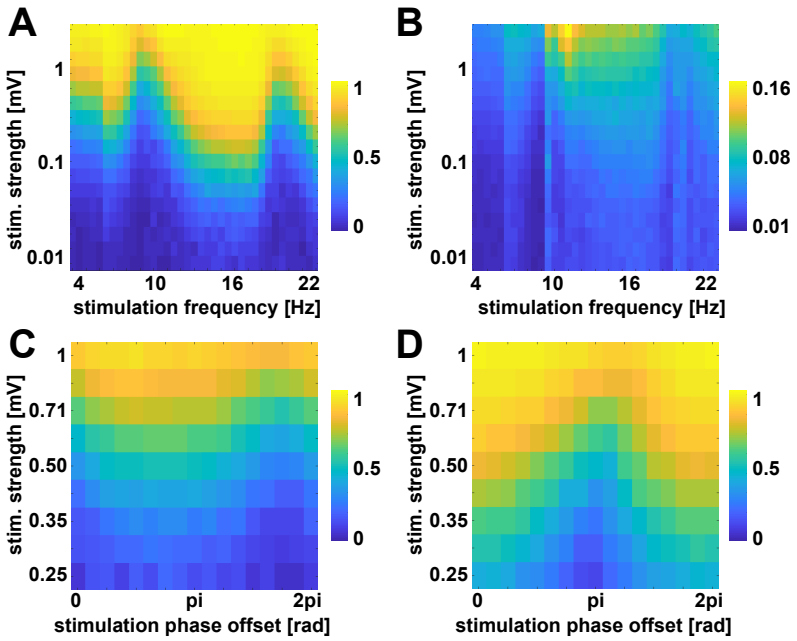

Figure 5. Stimulation parameter evaluation. (A) Coherence between the stimulus and the stimulated region for varying stimulus strength and frequency. The color corresponds to a mean value over 5 simulations at randomly chosen network nodes. (B) Coherence between the stimulus and the full network averaged over all 33 nodes for varying stimulus strength and frequency. The coherence was calculated between the stimulus and each region and then averaged. (C and D) Coherence between two stimulated nodes for varying stimulation strength and phase offset. C and D correspond to two different node pairs that were stimulated demonstrating the variability in phase lag preferences expressed by different pairs.

$(0 - 2\pi)$, while evaluating the coherence between the stimulated nodes. All other parameters were chosen to be the same as for the previous simulation. As can be seen in Figure 5C and Figure 5D, the variance of the coherence over phase offsets depended on the stimulation strength. Based on visual inspection of the coherence patterns of 20 different region pairs, we chose our stimulus scaling to be $c_{\text{ext}} = 0.5$ mV, leaving the variance of the post-synaptic potential of the neural masses in a biologically plausible range and such that the external driver is relatively weak in comparison to the internal network dynamics. This gave us the final set of global model parameters which were used throughout all subsequent simulations.

The variability in the coherence between stimulated region pairs that we observed not only over stimulation phase offsets but also over different pairs (as depicted for 2 exemplary region pairs in Figure 5C and 5D) shows that the stimulated region pairs interacted with each other and that the interactions showed a characteristic profile of phase offset preferences. To statistically confirm the variance in the coherence between stimulated region pairs over phase offsets, we ran simulations with stimulations of each possible node pair. Again, we varied the phase offset between the two stimuli (16 equally spaced phase offsets between 0 and 2π) and evaluated the coherence between the stimulated nodes for each phase offset. Subsequently, those coherences were used to calculate the PSF for each region pair as defined in equation 1. Using a one-sample t-test, we found the PSF effect to be significantly larger than zero (mean = 0.1567, CI = [0.1445,0.1689], t = 25.2595, p ¡ 0.0001). Hence, we were able to show with our

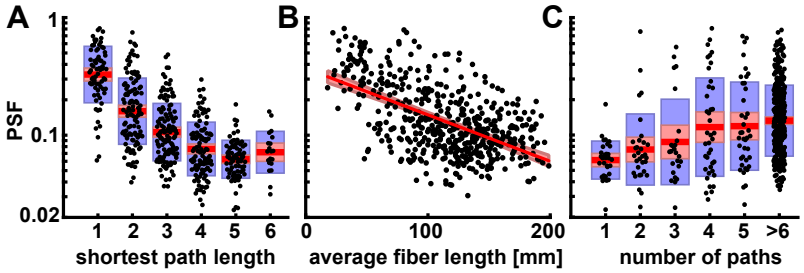

Figure 6. Pathway Synchronization Facilitation (PSF). All panels show the PSF on a logarithmic vertical axis and red areas indicate 95 % confidence intervals. Blue boxes indicate 1 standard deviation. (A) Dependence of PSF effect on shortest path length between the node pairs. (B) Correlation between PSF effect and average fiber length along the shortest pathway between the stimulated nodes. (C) Dependence of the PSF effect on the number of paths connecting the stimulated nodes.

extrinsic stimulation approach that pathways facilitated synchronization between cortical nodes and that the facilitatory strength depended on the phase lag between the region's average PSPs.

With the PSF effect established, we continued by investigating its dependence on certain features of the underlying structural connectivity graph. For this purpose, we searched for all possible pathways between each pair of stimulated nodes based on the structural connectivity matrix reported in Figure 4A. Since every stimulated pair of nodes was connected by at least one path via at most 6 edges, we restricted the search to pathways including 6 edges at maximum. With these pathways at hand, we started out by evaluating how the PSF effect changed with increasing network distance. An analysis of variance showed that the effect of shortest path length (minimum number of edges seperating a pair) on log(PSF) was significant, F(5,521) = 97.6141, p ¡ .0001. As can be seen in Figure 6A, we observed the trend that the PSF effect decreases with the number of nodes separating the stimulated nodes. Furthermore, as depicted in Figure 6B, this trend was supported by a significant correlation between the PSF effect and the length of the shortest pathway between the stimulated nodes (r = -0.56, p ¡ .0001), a measurement that is strongly related to both interregional distance and minimal number of separating edges. Thus, we conclude that there is a tendency for a decrease in the interaction of stimulated node pairs with increasing network distance between the nodes, where network distance can be measured either as the number of edges or as the summed up length of the edges of the shortest pathway connecting the nodes.

Next, we investigated the dependence of the PSF effect on the connectedness between the stimulated nodes. An analysis of variance showed that the effect of the number of connecting paths (only counting paths with 5 edges or less, all nodes with more than 5 connecting paths were pooled into one level) on log(PSF) was significant, F(5,501) = 10.0827, p ¡ .0001. The latter result can be observed in detail in Figure 6C.

Evaluation of Pathway Activation

Having described the influence of the external driver on the coherence between stimulated nodes, we next identified which particular pathways were involved in this interaction. For this analysis, we define the pathway activation (PA) for a pathway through n nodes k_i with $i = 1..n$ at a phase offset $\Delta\varphi$ as the minimum of the pairwise coherences between neighboring pathway nodes:

$$\mathrm{PA}(k_1..k_n, \Delta\varphi) = \min_{i=1,..,n-1} \Big(\mathrm{coh}(k_i, k_{i+1}, \Delta\varphi)\Big). \quad (2)$$

In other words, if communication fails at any point along a pathway, leading to a reduced coherence between the involved nodes, this is considered to be a bottleneck for the information flowing through that pathway. We evaluated the pathway activation (PA) 2 for all pathways of up to $n = 5$ nodes connecting a given pair of stimulated nodes for all stimulation phase offsets. Doing this for each stimulated node pair, we found different classes of pathway interactions: Some pairs show only a very small selectivity for the stimulation phase offset (Figure 7A), while other node pairs were connected by paths with PA values with a strong dependence on the phase offset (Figure 7B, 7C). Moreover, some of these node pairs switched their interaction between different pathways depending on the stimulation phase offset, as shown in Figure 7C and the two switching pathways in Figure 7D and 7E.

To further analyze how the communication via specific pathways depends on the stimulation phase offset, we define the pathway phase selectivity (PPS) of a pathway P_1 similar to the PSF as

$$\mathrm{PPS}(P_1) = \max_{\Delta\varphi}\big(\mathrm{PA}(P_1, \Delta\varphi)\big) - \min_{\Delta\varphi}\big(\mathrm{PA}(P_1, \Delta\varphi)\big), \tag{3}$$

Pathways with relatively constant PA values for all stimulation phase offsets have a low PPS (example in Figure 7A), while pathways with a high variation in the PA values have a high PPS (example in Figure 7B and 7C). The evaluation of PPS values for all node pairs results in a bimodal distribution (Figure 7F). The activation of pathways in the first mode at $PPS = 0.1$ is very hard to influence with phase offsets. But we also found many node pairs with pathways in the second mode at $PPS = 0.35$. The communication of these later node pairs can be modulated using different phase offsets.

In a next step, we analyzed the relationship of pathway-specific phase preferences (as shown in Figure 7A-C) to the phase preferences of the stimulated nodes (as shown in Figure 5C-D). We chose the most active pathway per node pair (averaged over all stimulation phase offsets) and calculated the phase difference between the stimulation phase offset with the highest coherence and the stimulation phase offset with the highest PA. The histogram of these phase differences is significantly different from uniform, $\chi^2(15, N = 514) = 273.05, p < .001$, and has a peak at 0 (Figure 7G). In contrast, a similar analysis for the second strongest pathway (excluding all pathways with overlapping sections with the strongest path), results in a histogram that does not differ from a uniform distribution, $\chi^2(15, N = 514) = 14.06, p = 0.52$ (Figure 7H). Therefore, we conclude that the pathway with the strongest PA shows a similar phase preference as the coherence between the two stimulated nodes.

Finally, we quantified the switching between the strongest and second strongest pathway per node pair. To this end, we define the pathway switching index (PSI) between pathways P_1 and P_2 as

$$\begin{aligned}\mathrm{PSI}(P_1, P_2) = &\max_{\Delta\varphi}\big(\mathrm{PA}(P_1, \Delta\varphi) - \mathrm{PA}(P_2, \Delta\varphi)\big) \\ &\cdot \max_{\Delta\varphi}\big(\mathrm{PA}(P_2, \Delta\varphi) - \mathrm{PA}(P_1, \Delta\varphi)\big),\end{aligned} \tag{4}$$

The PSI is positive if the two pathways switch their activation depending on the stimulation phase offset, meaning that at one phase offset the first path is more active and at another phase offset the second path is more active. We found that 60.1% (309 of 514) of node pairs have a positive PSI between their non-overlapping strongest and second strongest pathways (Figure 7I). These results suggest that in this network of 33 nodes of the human connectome many node pairs have the capacity to switch their communication between at least two different pathways with a PA characteristic similar to the example shown in Figure 7C.

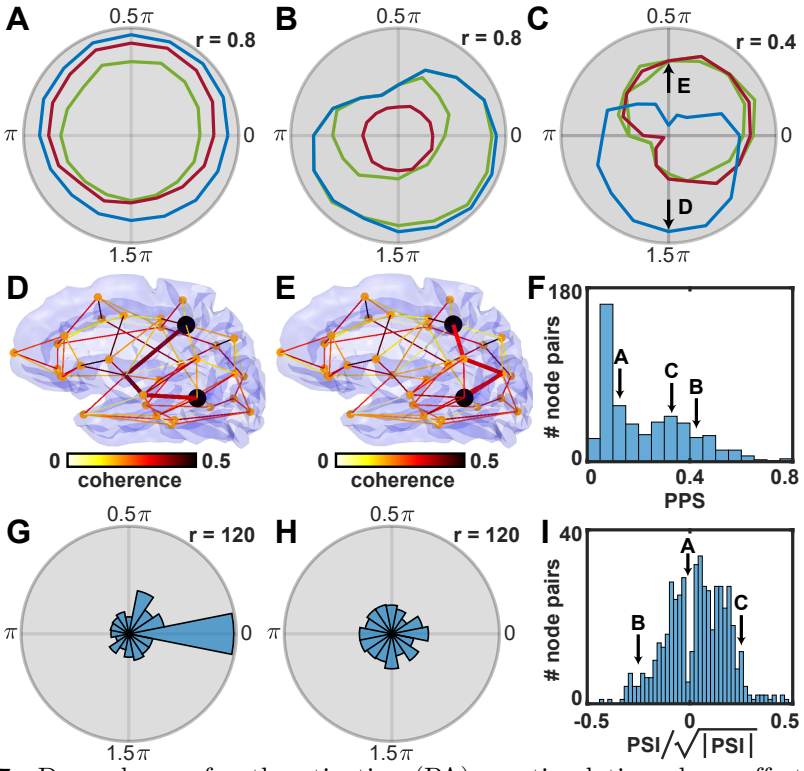

Figure 7. Dependence of path activation (PA) on stimulation phase offset. Panels (A-C) show the PA values (radius) for different stimulation phase offsets (angle) for exemplary node pairs. Blue corresponds to the pathway with the strongest overall PA. Red corresponds to the second strongest pathway that has no overlapping segments with the strongest. Green curves show the strongest of the remaining pathways (with possible overlapping path segments with the former two). The two arrows in (C) indicate the phase offsets which are used in panels (D-E). (D) Connectome pathways for stimulation of the node pair shown in (C) at phase offset 1.5π. The two stimulated nodes are shown as two black dots. The most active pathway at this stimulation phase offset is highlighted with a stronger line width. All colors correspond to the coherence of nearest neighbours in the connection graph. (E) Similar to (D) but for stimulation phase offset 0.5π with a different most active pathway. (F) Histogram of pathway phase selectivity. The values of the strongest paths of examples shown in (A-C) are marked with arrows. (G) Histogram of phase differences between the stimulation phase offset where the most active pathway has the highest pathway activation and the stimulation phase offset where the coherence between the stimulated nodes was highest. (H) Similar to (G) but for the second most active pathway (excluding path overlaps with the most active pathway). (I) Histogram of normalized pathway switching index between the strongest and second strongest pathways. The values of the node pairs of examples shown in (A-C) are marked with arrows. The square-root normalization of the PSI transforms back from the space of multiplied coherence values to the original non-squared coherence space (analogous to a transformation from variance to standard-deviation).

Discussion

We have carried a computational study of cortico-cortical synchronization processes that strongly emphasizes the role of phase relationships for dynamic switches in communication pathways. We introduced a novel method to detect network interactions

between pairs of cortical regions via an extrinsic stimulation scheme. Using our method, we were able to quantify the influence of different pathways on cortico-cortical synchronization processes between all pairs of 33 brain regions and could further identify the pathways those region pairs use to interact with each other. These pathways represent communication channels with distinct interaction time windows. We found the ability of regions to communicate via these channels to depend on the phase lag at which they try to synchronize [19]. This finding is in line with the communication-through-coherence theory that predicts neural communication to critically depend on oscillatory phase differences [16]. Furthermore, it provides a mechanistic explanation for the dependency of the effect of extrinsic brain stimulation on the stimulation phase [20] and could guide future brain stimulation studies that are investigating phase-lagged neural synchronization, e.g., through multi-site transcranial stimulation, or optogenetics in combination with multielectrode recordings [32]. Our method is also applicable in future theoretical studies characterizing the dynamic properties of network graphs.

Since we were further able to demonstrate that for different stimulation phase offsets between the communicating regions, different communication channels may be employed, we believe that the switching between different synchronization phase lags could be a potential mechanism through which brain regions can dynamically change their effective communication channels. As suggested in [11, 13], such a mechanism would provide the necessary flexibility to allow for the dynamic binding of remote neural representations into different concepts. Taken together, our results suggest a potential mechanism the human brain might have developed to use the physiological constraints imposed by coupling delays to its computational advantage.

Supporting Information

In the following, we present the detailed parameters of the neural mass model, the preprocessing of the structural connectivity, and the functional connectivity.

Neural Mass Model

All simulation results reported refer to 16 minutes of simulated network behavior, using an explicit Euler method with an integration step-size of 0.5 ms. The parameters of the neural mass model are shown in Table S1. To translate post-synaptic responses back into firing rates, the following instantaneous sigmoidal transform was used:

$$\sigma(V) = \frac{2e_0}{1 + e^{r(V_0 - V)}}. \tag{5}$$

Structural Connectivity and Distance Estimates

In a first step to building a bottom-up model of cortical activity we needed to approximate the structural connections between different brain regions. As mentioned in the introduction, this can be done via DTI recordings. However, there are several technical limitations as to what extend human SC can be approximated based on DTI, one of them being the systematic underestimation of inter-hemispheric connections [23, 31]. Thus we decided to restrict our analysis to the cerebral cortex of a single hemisphere. To this end, we used the same structural imaging data, pre-processing and probabilistic tracking pipeline as reported by Finger et al. [14], but restricted subsequent processing to the 33 regions of interest (ROIs) of the left hemisphere. This data set included diffusion- and T1-weighted images acquired from 17 healthy subjects (7 female, age mean = 65.6y ± 10.9y) with a 3 Tesla Siemens Skyra MRI scanner (Siemens, Erlangen, Germany) and a 32-channel head coil. The 33 ROIs were registered individually for each subject based on the 'Desikan-Killiany' cortical atlas available in the Freesurfer toolbox (surfer.nmr.mgh.harvard.edu) [10]. This gave us the euclidean distances between each pair of ROIs. The incoming connections to each region were normalized such that they summed up to 1. Since we were only interested in synchronization along indirect pathways, we needed some connections in our model to be strictly 0. Otherwise, it would be difficult to exclude potential synchronization along very weak direct connections. Hence, we chose to set all connections below a strength of 0.1 to zero. Afterwards, we re-normalized the input to each region such that they summed up to 1. The resulting SC matrix as well as the pair-wise distances are visualized in Figure 4A and 4B in the main paper.

Empirical Resting-State Functional Connectivity

Based on those SC and distance information we aimed to build a model of cortical activity able to reflect empirically observed synchronization behavior. Thus we needed empirical observations of cortical activity to evaluate our model. For this purpose, we acquired EEG data from the same 17 subjects as described above. This was done with 63 cephalic active surface electrodes arranged according to the 10/10 system (actiCAP R Brain Products GmbH, Gilching, Germany) for eight minutes of eyes-open resting-state. Again, data acquisition and pre-processing followed the same procedure as reported by Finger et al. [14]. EEG time-series from the surface electrodes were projected onto the centers of the ROIs via a linear constraint minimum variance spatial beam former [30]. The resulting source-space signals were band-pass filtered at 10 Hz and turned into analytic signals using the Hilbert transform. Subsequently, functional connectivity was evaluated as the coherence between all pairs of ROIs [1]. This resulted

in the 33 x 33 functional connectivity matrix that can be observed in Figure 4C in the main paper and served as optimization target for our model.

Table S1. Model Parameters

Param.	Value	Interpretation
H_e	3.25 mV	avg. gain of excitatory synapses
H_i	22 mV	avg. gain of inhibitory synapses
τ_e	10 ms	lumped time constant of excitatory synapses
τ_i	20 ms	lumped time constant of inhibitory synapses
κ_1	135	avg. number of contacts from EINs to PCs
κ_2	$0.8\kappa_1$	avg. number of contacts from IINs to PCs
κ_3	$0.25\kappa_1$	avg. number of contacts from PCs to EINs
κ_4	$0.25\kappa_1$	avg. number of contacts from PCs to IINs
e_0	2.5 Hz	maximum scaling of the synaptic gain
r	0.56 mV^{-1}	steepness of the sigmoid function
v_0	6 mV	value with 50% of max. firing rate
μ_u	120 - 320 Hz	sub-cortical input
dt	0.5 ms	simulation step size

Acknowledgments

This research has been funded by the DFG (SFB 936, projects A2/A3/C1/Z1).

References

1. C. Andrew and G. Pfurtscheller. Event-related coherence as a tool for studying dynamic interaction of brain regions. *Electroencephalography and Clinical Neurophysiology*, 98(2):144–148, 1996.

2. M. J. Brookes, J. R. Hale, J. M. Zumer, C. M. Stevenson, S. T. Francis, G. R. Barnes, J. P. Owen, P. G. Morris, and S. S. Nagarajan. Measuring functional connectivity using meg: methodology and comparison with fcmri. *NeuroImage*, 56(3):1082–1104, 2011.

3. J. Cabral, E. Hugues, O. Sporns, and G. Deco. Role of local network oscillations in resting-state functional connectivity. *NeuroImage*, 57(1):130–139, 2011.

4. J. Cabral, M. L. Kringelbach, and G. Deco. Functional connectivity dynamically evolves on multiple time-scales over a static structural connectome: Models and mechanisms. *NeuroImage*, 2017.

5. V. D. Calhoun, K. A. Kiehl, and G. D. Pearlson. Modulation of temporally coherent brain networks estimated using ica at rest and during cognitive tasks. *Human Brain Mapping*, 29(7):828–838, 2008.

6. J. Damoiseaux, S. Rombouts, F. Barkhof, P. Scheltens, C. Stam, S. M. Smith, and C. Beckmann. Consistent resting-state networks across healthy subjects. *Proceedings of the National Academy of Sciences*, 103(37):13848–13853, 2006.

7. G. Deco and M. Corbetta. The dynamical balance of the brain at rest. *The Neuroscientist*, 17(1):107–123, 2011.

8. G. Deco, V. K. Jirsa, and A. R. McIntosh. Emerging concepts for the dynamical organization of resting-state activity in the brain. *Nature Reviews Neuroscience*, 12(1):43, 2011.

9. G. Deco, M. L. Kringelbach, V. K. Jirsa, and P. Ritter. The dynamics of resting fluctuations in the brain: metastability and its dynamical cortical core. *Scientific Reports*, 7(1):3095, 2017.

10. R. S. Desikan, F. Ségonne, B. Fischl, B. T. Quinn, B. C. Dickerson, D. Blacker, R. L. Buckner, A. M. Dale, R. P. Maguire, B. T. Hyman, et al. An automated labeling system for subdividing the human cerebral cortex on mri scans into gyral based regions of interest. *NeuroImage*, 31(3):968–980, 2006.

11. A. K. Engel, C. Gerloff, C. C. Hilgetag, and G. Nolte. Intrinsic coupling modes: multiscale interactions in ongoing brain activity. *Neuron*, 80(4):867–886, 2013.

12. A. K. Engel, P. König, A. K. Kreiter, T. B. Schillen, and W. Singer. Temporal coding in the visual cortex: new vistas on integration in the nervous system. *Trends in Neurosciences*, 15(6):218–226, 1992.

13. A. K. Engel and W. Singer. Temporal binding and the neural correlates of sensory awareness. *Trends in Cognitive Sciences*, 5(1):16–25, Jan. 2001.

14. H. Finger, M. Bönstrup, B. Cheng, A. Messé, C. Hilgetag, G. Thomalla, C. Gerloff, and P. König. Modeling of large-scale functional brain networks based on structural connectivity from dti: comparison with eeg derived phase coupling networks and evaluation of alternative methods along the modeling path. *PLoS Computational Biology*, 12(8):e1005025, 2016.

15. M. D. Fox, A. Z. Snyder, J. L. Vincent, M. Corbetta, D. C. Van Essen, and M. E. Raichle. The human brain is intrinsically organized into dynamic, anticorrelated functional networks. *Proceedings of the National Academy of Sciences*, 102(27):9673–9678, 2005.

16. P. Fries. Rhythms for Cognition: Communication through Coherence. *Neuron*, 88(1):220–235, Oct. 2015.

17. M. D. Greicius, B. Krasnow, A. L. Reiss, and V. Menon. Functional connectivity in the resting brain: a network analysis of the default mode hypothesis. *Proceedings of the National Academy of Sciences*, 100(1):253–258, 2003.

18. J. Gross, F. Schmitz, I. Schnitzler, K. Kessler, K. Shapiro, B. Hommel, and A. Schnitzler. Modulation of long-range neural synchrony reflects temporal limitations of visual attention in humans. *Proceedings of the National Academy of Sciences*, 101(35):13050–13055, 2004.

19. G. Hahn, A. Ponce-Alvarez, G. Deco, A. Aertsen, and A. Kumar. Portraits of communication in neuronal networks. *Nature Reviews Neuroscience*, page 1, 2018.

20. R. F. Helfrich, T. R. Schneider, S. Rach, S. A. Trautmann-Lengsfeld, A. K. Engel, and C. S. Herrmann. Entrainment of brain oscillations by transcranial alternating current stimulation. *Current Biology*, 24(3):333–339, 2014.

21. B. H. Jansen and V. G. Rit. Electroencephalogram and visual evoked potential generation in a mathematical model of coupled cortical columns. *Biological Cybernetics*, 73(4):357–366, 1995.

22. P. König and T. B. Schillen. Stimulus-dependent assembly formation of oscillatory responses: I. synchronization. *Neural Computation*, 3(2):155–166, 1991.

23. L. Li, J. K. Rilling, T. M. Preuss, M. F. Glasser, F. W. Damen, and X. Hu. Quantitative assessment of a framework for creating anatomical brain networks via global tractography. *NeuroImage*, 61(4):1017–1030, 2012.

24. D. Mantini, M. G. Perrucci, C. Del Gratta, G. L. Romani, and M. Corbetta. Electrophysiological signatures of resting state networks in the human brain. *Proceedings of the National Academy of Sciences*, 104(32):13170–13175, 2007.

25. A. Messé, D. Rudrauf, A. Giron, and G. Marrelec. Predicting functional connectivity from structural connectivity via computational models using mri: an extensive comparison study. *NeuroImage*, 111:65–75, 2015.

26. M. E. Raichle. The brain's default mode network. *Annual Review of Neuroscience*, 38:433–447, 2015.

27. S. L. Schmidt, A. K. Iyengar, A. A. Foulser, M. R. Boyle, and F. Fröhlich. Endogenous cortical oscillations constrain neuromodulation by weak electric fields. *Brain Stimulation*, 7(6):878–889, 2014.

28. M. Siegel, T. H. Donner, and A. K. Engel. Spectral fingerprints of large-scale neuronal interactions. *Nature Reviews Neuroscience*, 13(2):121, 2012.

29. M. P. Van Den Heuvel and H. E. H. Pol. Exploring the brain network: a review on resting-state fmri functional connectivity. *European Neuropsychopharmacology*, 20(8):519–534, 2010.

30. B. D. Van Veen, W. Van Drongelen, M. Yuchtman, and A. Suzuki. Localization of brain electrical activity via linearly constrained minimum variance spatial filtering. *IEEE Transactions on Biomedical Engineering*, 44(9):867–880, 1997.

31. V. J. Wedeen, R. Wang, J. D. Schmahmann, T. Benner, W.-Y. I. Tseng, G. Dai, D. Pandya, P. Hagmann, H. D'Arceuil, and A. J. de Crespigny. Diffusion spectrum magnetic resonance imaging (dsi) tractography of crossing fibers. *NeuroImage*, 41(4):1267–1277, 2008.

32. A. Yazdan-Shahmorad, D. B. Silversmith, V. Kharazia, and P. N. Sabes. Targeted cortical reorganization using optogenetics in non-human primates. *eLife*, 7:e31034, 2018.